BILINGUAL PUBLISHING GROUP

Journal of Building Material Science
https://journals.bilpubgroup.com/index.php/jbms

ARTICLE

Thermal Behavior Analysis of Natural Composites Materials Comprising Diatomaceous Earth and Sugarcane Bagasse

William Villarreal , ***Lucio Llontop*** , ***Alberto Hananel*** *

Faculty of Engineering, Santo Toribio de Mogrovejo Catholic University, Chiclayo, Lambayeque 14001, Peru

ABSTRACT

This work quantifies the thermal performance of natural composite blocks made from Yapatera diatomaceous earth reinforced with sugarcane bagasse fibres. Prismatic specimens (185 × 185 mm) with three thicknesses (≈76 mm, 100 mm, and 150 mm) and bagasse contents of 5–15% (wt.) were tested at hot-face temperatures of 100, 250, and 450 °C in a full-factorial 3 × 3 × 3 plan (54 tests). Thermal conductivity (k) was measured using a guarded hot-plate device aligned with ASTM D5470/E1530/C177. The measured k averaged 0.125 W/m·K (range ~0.088–0.220 W/m·K) and remained stable in function up to 500 °C. ANOVA showed that temperature and thickness significantly increased k ($p < 0.05$), while fibre content had a weaker, non-monotonic effect beyond ~10%. A response-surface model (RSM) provided accurate predictions ($R^2 \approx 0.95$). For design purposes, thermal resistance was computed as $R = \frac{\Delta x}{k}$. A 150 mm block yielded R ≈ 1.20 m^2K/W, comparable to ~0.40 m of hollow ceramic brick and > 1.0 m of concrete to reach a similar R. The composite therefore occupies a distinct niche: medium-performance insulation with high-temperature stability (≤ 500 °C), low embodied energy (air-dried manufacturing, agro-waste feedstock), and competitive cost potential. These results support its use in industrial and building applications where conventional insulators are unsustainable or operate below the required temperature window.

Keywords: Diatomaceous Earth; Sugarcane Bagasse; Thermal Conductivity; Thermal Resistance; Sustainable Insulation; Response Surface Methodology

*CORRESPONDING AUTHOR:
Alberto Hananel, Faculty of Engineering, Santo Toribio de Mogrovejo Catholic University, Chiclayo, Lambayeque 14001, Peru; Email: ahananel@usat.edu.pe

ARTICLE INFO
Received: 7 August 2025 | Revised: 19 August 2025 | Accepted: 8 September 2025 | Published Online: 18 September 2025
DOI: https://doi.org/10.30564/jbms.v7i3.11522

CITATION
Villarreal, W., Llontop, L., Hananel, A., 2025. Thermal Behavior Analysis of Natural Composites Materials Comprising Diatomaceous Earth and Sugarcane Bagasse. Journal of Building Material Science. 7(3): 183–205. DOI: https://doi.org/10.30564/jbms.v7i3.11522

1. Introduction

In industrial thermal systems and refrigeration applications, minimising heat losses to the environment is essential for enhancing energy efficiency, reducing operational costs, and mitigating greenhouse gas emissions. Thermal insulation is crucial in this context, achieved by introducing materials with low thermal conductivity between a heat source and its surroundings to impede the transfer of energy via conduction, convection, or radiation [1–4].

According to Bahadori [5], a material is considered a good thermal insulator when its thermal conductivity remains below approximately 0.05 W/(m·K), or when its thermal resistance exceeds 0.25 m2·K/W. Conventional insulating materials include fibreglass, mineral wool, vermiculite, calcined diatomite, and polymer foams such as polystyrene and polyurethane, with conductivities in the range of 0.03—0.06 W/(m·K) [6,7]. Despite their widespread use, these materials present drawbacks such as high embodied energy, susceptibility to moisture and chemical degradation, diminished thermal performance at elevated temperatures, and potential health concerns linked to particulate emissions and indoor air quality [8,9].

Recent research has increasingly focused on sustainable, bio-based alternatives. Lignocellulosic resources, such as recycled cellulose fibres, cork, rice husks, coconut husk, and sugarcane bagasse, have shown promising insulating properties, often achieving conductivities of 0.04—0.07 W/(m·K), comparable to synthetic foams [10–12]. Their microstructural features—including fibre orientation, porosity, and moisture content—strongly influence heat transfer pathways and effective conductivity [13,14]. Additionally, fibre treatments and tailored processing can improve mechanical performance while maintaining low thermal conductivity [15,16].

Mineral-based materials also remain relevant in sustainable insulation. Diatomaceous earth (diatomite), a siliceous sedimentary rock composed of fossilised diatoms, offers high porosity and low density, translating into intrinsically low thermal conductivity values of 0.05–0.07 W/(m·K) [17–19]. Although commonly used in filtration and as an additive in refractories, its use in monolithic insulating blocks is limited, largely due to weak cohesion in loose form [20,21]. Stabilisation strategies—such as integrating diatomite with organic or mineral binders—have demonstrated potential to enhance both mechanical integrity and thermal efficiency [22,23].

Sugarcane bagasse, a by-product of sugar production in regions such as northern Peru, represents an abundant lignocellulosic resource. Its composition (cellulose, hemicellulose, and lignin) promotes low density and high porosity, which interrupts conductive pathways by trapping stagnant air within pores [24–26]. When combined with diatomite, these properties support the development of low-cost, eco-friendly composites suitable for thermal insulation in construction [27,28].

Research Objective: This research aims to evaluate the effective thermal conductivity of composite blocks made from diatomaceous earth and sugarcane bagasse. The study analyses the influence of temperature, thickness, and fibre concentration on thermal behaviour through a factorial design and analysis of variance (ANOVA), complemented by Response Surface Methodology (RSM), to determine optimal composition and performance. Because porosity is a primary factor governing heat retention in composites, we also clarify the forming procedure that controls pore uniformity: the fresh mix was poured into wooden moulds and compacted manually with a metallic rammer until the mould was filled and levelled. This protocol was chosen to remove large air voids and ensure homogeneous filling; however, no controlled pressing was applied to systematically change density. The identical compaction routine was executed by the same operator for all specimens to promote comparable porosity across samples. This artisanal, low-energy route aligns with a circular-economy perspective; nevertheless, future work should employ a hydraulic press to impose specific, reproducible pressures, enabling a quantitative study of the compaction—porosity—conductivity relationship.

2. Materials and Methods

2.1. Materials

The diatomaceous earth used was extracted from the Yapatera deposits (Morropón province, Piura, Peru). Its typical chemical composition is shown in **Table 1**, highlighting a high content of silica (~62%) and alumina

(~33%), along with small proportions of iron, calcium, magnesium, and alkali oxides. The material appears as a fine, light beige powder derived from siliceous fossiliferous sedimentary rock.

Table 1. Chemical composition of the Yapatera soil.

Chemical Composition	Percentage (%)
Al_2O_3	33.00
SiO_2	62.00
Fe_2O_3	2.50
CaO + MgO	1.00
$Na_2O + K_2O$	1.50

Source: Organics AgroYap SAC (https://www.facebook.com/OrganicosAgroYap?_rdc=1&_rdr#)

The sugarcane bagasse was sourced from a local sugar mill; prior to use, it was air-dried and coarsely ground. **Table 2** summarises the approximate composition of the dry bagasse: it is composed of 40% cellulose (main plant fibres), ~25% hemicellulose, ~20–30% lignin (structural cell wall components), as well as ~5–9% sugars and traces of inorganic ash. Both materials (diatomaceous earth and bagasse fibre) were considered suitable for formulating a 100% natural composite material without chemical additives.

Table 2. Physical composition of sugarcane bagasse.

Physical Component	Percentage (%)
Cellulose	38.40–45.50
Hemicellulose	22.70–27.00
Lignin	19.10–32.40
Ash	1.00–2.80
Sugars and impurities	4.60–9.10

Source: Rein [24].

2.2. Sample Preparation

Square prismatic blocks (solid panel type) were fabricated by mixing diatomaceous earth with bagasse fibre and water in a 3:2:1 volume ratio (equivalent to approximately 3 parts earth, 2 parts bagasse, and 1 part water, due to the fibre's low density). The blended mixture was placed into wooden moulds of 185×185 mm cross-section, producing plate-shaped specimens. Three nominal block thicknesses were prepared: ~76 mm (≈3"), 100 mm (4"), and 150 mm (6"). To prevent cracking during setting, the blocks were air-dried in the shade for five days and demoulded once hardened. Afterwards, the samples were stored in a dry laboratory environment until testing, to prevent reabsorption of ambient moisture.

The specimens were visually inspected before testing and found to be apparently dry, with no evidence of surface moisture. The blocks had remained outdoors for three weeks prior to laboratory reception, which was considered sufficient for natural drying. In line with internal laboratory protocols, the Peruvian building standards RNE E.070–E.080 for adobe bricks, and ASTM D2216-19 (moisture content in soils), oven-drying was deemed unnecessary in this initial characterisation since no free moisture was detected. Nevertheless, the possibility of residual bound water within the porous diatomite–bagasse matrix cannot be excluded. For this reason, future tests will implement controlled oven drying and desiccator storage to fully eliminate moisture effects and to allow more direct comparisons with reference materials in the literature.

2.3. Experimental Design

The effect of three independent variables on the thermal conductivity of the composite material was studied:

- Temperature of the hot surface of the block (°C): levels of 100, 250, and 450 °C.
- Block thickness (mm): levels of 76, 100, and 150 mm.
- Bagasse fibre content (weight % of the dry block): levels of 5%, 10%, and 15%.

A full factorial 3×3×3 design was applied, with two replicates per combination, resulting in 54 experimental tests in total. The combinations of factors were randomly assigned and tested to ensure observation independence and avoid systematic bias. This number of experiments (N = 54) provides sufficient degrees of freedom for robust ANOVA and the estimation of interaction terms. Prior to the tests, the null hypothesis was stated as: none of the variables (temperature, thickness, bagasse content) has a significant effect on the composite's thermal conductivity; against the alternative hypothesis that at least one variable does exert influence. A significance level of $\alpha = 0.05$ (95% confidence) was adopted for the statistical tests.

The full factorial design and subsequent statistical analyses were implemented using Statistica (TIBCO Software Inc.), MATLAB R2023a (MathWorks Inc.), Design-Expert

13 (Stat-Ease Inc.), and Minitab 21 (Minitab LLC). For transparency and reproducibility, a summary of the DOE matrix is provided in **Table 3**, while the complete set of 54 experimental runs is presented in **Appendix A** (**Table A1**).

Table 3. Full factorial 3 × 3 × 3 DOE matrix (extract). The complete 54 runs are provided in Appendix A.

Exp.	Temp. (°C)	Thick. (mm)	Bagasse (%)	k (W/m·K)
1	100	76	5	0.0845
2	250	76	5	0.0881
3	450	76	5	0.1194
...	...	...	...	...
54	450	150	15	0.1808

2.4. Apparatus and Test Procedure

Figure 1 illustrates the solid samples prepared in the form of square prismatic blocks, ready for testing. To measure the thermal conductivity of the blocks indirectly (via Fourier's law), an experimental setup was designed based on the guarded hot plate method. The sample was placed between a controlled heat source and a cooling system so that the heat flux passed through the block thickness in a nearly unidirectional and steady-state manner.

Figure 2 shows the electronic and electromechanical instruments used to impose the thermal gradient and record temperature and heat flux.

Figure 1. Square prismatic block samples.

(**a**) (**b**)

Figure 2. (**a**) Electronic and electromechanical instrumentation for recording temperature, voltage, and current during the thermal test; and (**b**) Thermal-insulated press fixture with integrated sensors and heating-cooling system for the evaluation of composite blocks.

The main equipment used was as follows:

- **Heat Source:** An 800 W electric resistance heating element (approx. 130 Ω) coupled to a 185 × 185 mm hot metal plate. Additionally, an oxyacetylene torch directed at a steel plate was used to reach higher temperature levels.
- **Cooling System:** A 300 × 300 mm cooling plate with internal channels, connected to a water circuit at 20 °C (inlet and outlet through 3/4" pipes). To ensure effective cooling, a continuous high flow rate of approximately 0.15 L/s was maintained. This prevented any significant temperature rise of the coolant, maximised the convective heat transfer coefficient, and ensured that the dominant thermal resistance corresponded to the tested block.
- **Fixing System:** A mechanical press with jaws firmly holding the block during the test (**Figure 2b**). The hot jaw includes the heating element, and the cold jaw integrates the water cooling chamber. All exposed faces of the block (except those in contact with the plates) were externally insulated with mineral wool to force unidirectional heat flow across the sample thickness.
- **Measuring Instrumentation:** Type K thermocouples (steel capsule, 5 × 50 mm) and digital data acquisition. Nine thermocouples were installed in each test: three placed near the hot surface of the block (approx. 10 mm below the hot face, evenly distributed), three near the cold surface (approx. 10 mm above the cold face), and three along the sides of the block. Thermocouples were inserted into ~2.5 mm diameter perforations to a depth of ~50 mm to ensure good internal thermal contact. In addition, the system included: 2 microcontrollers, 2 digital displays, 1 data logger for graph recording, 1 multi-channel acquisition system, and 1 voltage regulator (0–120 V) to adjust the power supplied to the resistance heater. Voltage and current supplied to the resistance were continuously monitored, allowing the calculation of the heat flux (q) through the sample using the equation q = VI/A (product of voltage and current divided by the sample cross-sectional area).

It is important to emphasise that the homogeneous distribution of the mixture inside the moulds led to the formation of pores of relatively uniform size. These pores, filled with static air, act as heat-retaining channels and are the primary contributors to the measured thermal conductivity, since they interrupt solid conduction paths. Because the compaction and distribution protocol was identical for all specimens, pore structure remained consistent across all tests.

The cooling water circulation was continuously monitored by measuring inlet and outlet temperatures (Twater,in and Twater,out). The heat removed by the cooling system was quantified as:

$$Q = m.cp\ (Tout - Tin\ ),$$

where m. is the water mass flow rate (kg/s), cp is the specific heat of water (J/kg·K), and (Tout − Tin) is the measured temperature difference. Under steady-state conditions, this Q matched both the electrical input (Q = VI) and the Fourier conduction model across the block, confirming the consistency and validity of the test method.

Each test was conducted as follows: the block was mounted in the press fixture to ensure uniform contact on both faces. The cold-side water flow was activated first, maintaining ~20 °C, and heating was gradually applied to the hot side until the target temperature (100, 250, or 450 °C) was reached. Steady state was defined as the condition where temperature readings varied by less than ±1 °C over a 10-minute interval ($dT/dt \approx 0$). Stabilisation times were typically ~4 hours at 450 °C and shorter at lower temperatures or thinner blocks. During the transient phase, data were collected every 5 to 10 minutes, while at steady state, at least three consecutive readings were taken at 10-minute intervals and averaged. After each test, the block was allowed to cool naturally, and the plates were cleaned before the next run. A minimum of 5 hours was allowed between tests to ensure baseline recovery of the apparatus. he test order was randomised to avoid systematic bias.

2.5. Microstructural Analysis

Advanced techniques such as scanning electron microscopy (SEM) or mercury intrusion porosimetry were not available for this study due to technical and budgetary constraints. As an alternative, a stereoscopic microscope (Stemi 508, Zeiss) was employed to preliminarily examine the surface microstructure of the bagasse-modified bricks prior to thermal exposure. Representative stereoscopic

micrographs are shown in **Figures 3** and **4**, which reveal pores, cracks, and surface irregularities associated with both the fabrication process and the fibre inclusion. The measured crack widths ranged from 216.31 µm to 802.44 µm, as documented in the images. These observations provide qualitative baseline evidence of the material's initial state, serving as a reference for future analyses aimed at identifying structural changes after thermal treatment. Although SEM or porosimetry would enable a more detailed and quantitative characterisation, stereoscopic microscopy provided consistent visual evidence in line with approaches previously applied to ceramic and refractory materials [29,30].

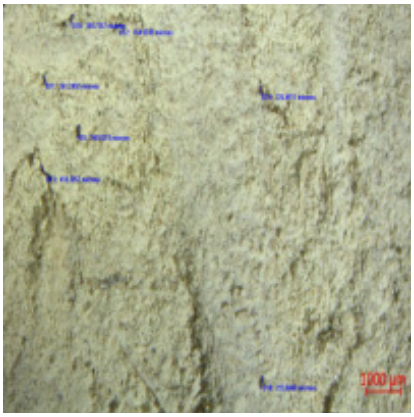

Figure 3. Stereoscopic micrograph of the bagasse-modified brick prior to thermal treatment, showing visible pores and cracks.

Figure 4. Detailed stereoscopic micrograph highlighting crack widths (ranging between 216.31 µm and 802.44 µm) and porosity distribution in the composite.

2.6. Calculation of Thermal Conductivity

A one-dimensional steady-state heat conduction model was assumed across the sample, neglecting interfacial thermal resistances (firm contact and thermal paste were applied to improve the interface; interfacial resistance was considered negligible). Under these conditions, thermal conductivity (k) was calculated based on Fourier's law in one dimension:

$$q = -kA\frac{\Delta T}{\Delta x}$$

where q is the heat flux (W) passing through area A (m^2) of the block, and $\Delta T/\Delta x$ is the temperature gradient in the direction of heat flow (°C/m). Rearranging gives:

$$k = -\frac{q\Delta x}{A\Delta T}$$

where Δx is the sample thickness and $\Delta T = T_{hot} - T_{cold}$ is the temperature difference between the hot and cold faces in steady-state conditions. In each trial, q was determined from the electrical power input (neglecting lateral losses due to external insulation), A was constant ($0.185 \times 0.185 = 0.0342\ m^2$), Δx was the nominal thickness

of the sample, and ΔT was derived from the thermocouple readings close to each surface.

Additionally, thermal resistance was also calculated as:

$$R = \frac{e}{k}$$

where e is the specimen thickness (m) and k the measured thermal conductivity (W/m·K). This parameter provides direct insight into the insulating ability of the blocks and allows comparison with commercial materials.

The compacting pressure applied during block preparation was estimated as:

$$F = Pgh \times A,$$

where P is the density of the material (kg/m^3), g is the gravitational acceleration (9.81 m/s^2), h is the compaction height (m), and A is the surface area of the mould (m^2).

Porosity (ε) was determined by:

$$\varepsilon = 1 - \frac{\rho_b}{\rho_s}$$

where Pb is the bulk density and Ps is the solid density of the material. This parameter quantifies the fraction of void space within the composite, which directly influences thermal conductivity.

Additionally, a simplified transient model was employed to estimate the temporal variation of temperature within the block during the heating and cooling phases (based on Newton's exponential cooling equation and the concept of thermal diffusivity), although the main analysis focused on steady-state thermal conductivity values.

The experimental procedure followed for thermal conductivity measurement was based on recommendations from ASTM D5470, ASTM E1530, and ASTM C177-19, adapted to the sample size and temperature range in this study. These standards establish reference methods for measuring heat transfer properties in solid materials, providing confidence in the validity of the results obtained.

2.7. Statistical Analysis

Using the thermal conductivity values calculated for each of the 54 tests, a three-way ANOVA was performed to assess the significance of the effect of each factor (temperature, thickness, and bagasse content) and their interactions on the response variable k. The assumptions of normality and homogeneity of variances were verified on the residuals prior to interpreting the F- and p-statistics. Effects with a *p*-value < 0.05 (95% confidence) were considered statistically significant.

Furthermore, Response Surface Methodology (RSM) was employed to model thermal conductivity as a polynomial function of the independent variables. A second-order (quadratic) regression model was fitted, including linear, quadratic, and bilinear interaction terms. For response surface construction, a Box-Behnken design with three factors (temperature, thickness, bagasse) requiring 15 base experimental runs was originally considered; however, since the full factorial design of 27 points covered the entire experimental space, all data were used to fit a more robust model.

Finally, although not part of the original experimental scope, the importance of techno-economic feasibility was highlighted. In future work, a break-even point analysis will be conducted using the following relation to determine the economic competitiveness of the proposed material compared with commercially available insulating bricks.

$$BEP = \frac{\text{Fixed Costs}}{\text{Selling Price} - \text{Variable Cost}}$$

This analysis, together with other financial indicators (NPV, IRR), will support the transition of the present research from laboratory validation to industrial application.

3. Results

3.1. Average Properties and Variability

The average thermal conductivity value obtained for diatomaceous earth mixed with bagasse (considering all tests) was approximately 0.125 W/(m·K). This value falls within the typical range for medium-density mineral insulating materials. **Table 4** summarises the mean conductivity results for each combination of factors (27 unique combinations, each averaged over two replicates).

Table 4. Average thermal conductivity results [W/(m·°C)] as a function of heating temperature, block thickness, and percentage of sugarcane bagasse fibres.

Thickness (m)	Temperature (°C)	Thermal Conductivity, W/(m·°C)											
		5%			10%			15%			20%		
		100	250	450	100	250	450	100	250	450	100	250	450
3”	100	0.0845	0.0881	0.1194	0.0495	0.0698	0.0950	0.0924	0.1388	0.1512	-	-	-
	250	0.0761	0.0978	0.1070	0.0554	0.0718	0.1064	0.1072	0.1512	0.1387			
4”	100	0.0943	0.1012	0.1137	0.1706	0.1341	0.1578	0.1172	0.1228	0.1350	-	-	-
	250	0.0849	0.0912	0.1202	0.1372	0.1490	0.1488	0.1075	0.1338	0.1472			
6”	100	0.1120	0.1184	0.1896	0.1354	0.1381	0.2030	0.1340	0.1678	0.1659	0.1839	0.0746	0.2100
	250	0.1025	0.1326	0.1916	0.1745	0.1498	0.2294	0.1229	0.1824	0.1808	0.2200	0.2078	0.2068

A considerable spread was observed in the individual k values, ranging from a minimum of ~0.088 W/(m·K) to a maximum of ~0.220 W/(m·K). This variability reflects the significant influence of the test conditions (levels of each factor) on the measured thermal conductivity, exceeding mere experimental random variation. In other words, the differences between treatments are statistically significant, as later confirmed by the analysis of variance.

The ability to obtain such distinct k values under different combinations confirms that the experimental design was appropriate for capturing the dependency of conductivity on temperature, thickness, and fibre content.

3.2. Effect of Temperature and Thickness

In general terms, it was found that increasing the temperature of the hot wall tends to raise the effective thermal conductivity of the block. This can be seen in **Figure 5**, where the average k coefficient is plotted as a function of temperature for different thicknesses.

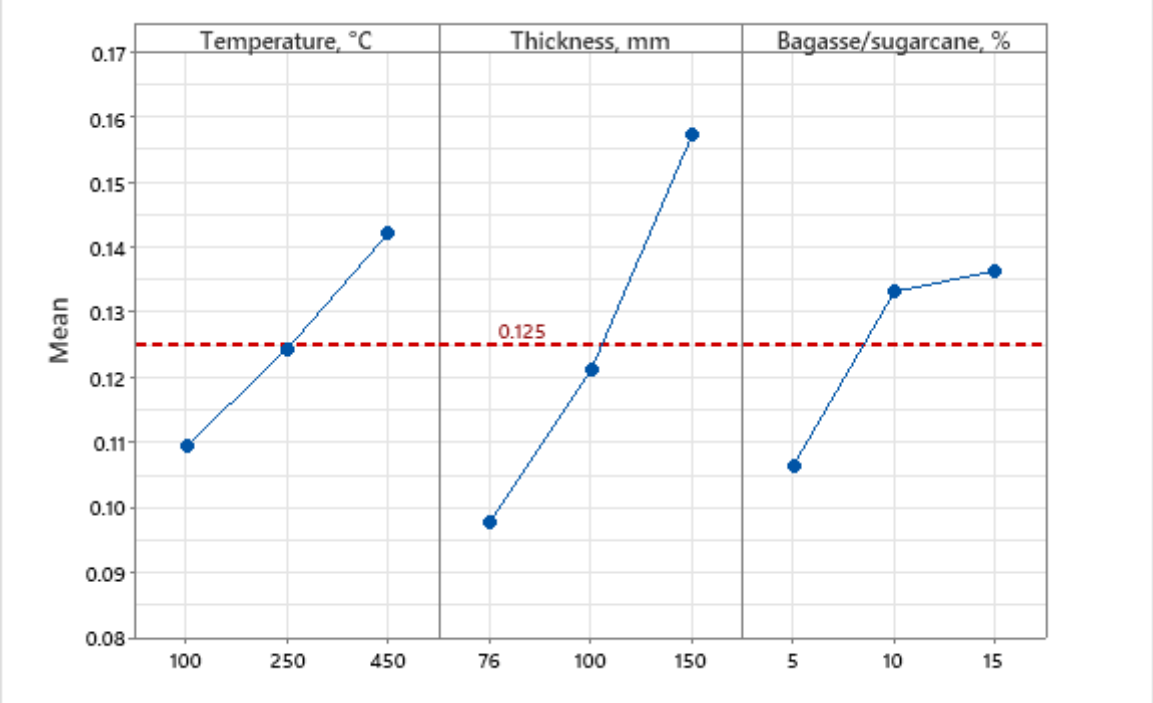

Figure 5. Effect of heating surface temperature, block thickness, and bagasse content on the average thermal conductivity of the composite material.

For example, keeping the thickness fixed at 150 mm, increasing the temperature from 100°C to 450°C raised k from approximately 0.10 to ~0.20 W/m·K. Likewise, greater material thickness resulted in higher apparent thermal conductivity, especially at elevated temperatures.

Figure 5 shows that the k vs. temperature curves for thicknesses of 76 mm, 100 mm, and 150 mm all have positive slopes and are clearly separated: the thinnest sample consistently shows the lowest conductivity across the temperature range, while the thickest one exhibits the highest k values. At the extreme point of 450 °C, the 150 mm block reached the maximum measured conductivity (~0.22 W/m·K), compared to ~0.12 W/m·K for the 76 mm block.

It is worth noting that at 100°C, the differences due to thickness were smaller (converging towards ~0.08–0.10 W/m·K). This suggests that the effect of thickness becomes more pronounced at higher temperatures. One possible explanation is that in thicker blocks, less uniform internal temperature gradients or minor internal convection may increase heat transfer under high temperatures.

However, since k is an intensive property of the material, it should ideally not depend on geometric dimensions. Therefore, this result indicates that experimental factors such as thermal contact resistance, transient gradients, or heterogeneities in fibre distribution may have influenced the measurements in very thick blocks.

Nevertheless, the observed trend is clear: higher temperatures and thicker specimens lead to greater effective thermal conductivity values in this composite material.

3.3. Effect of Fibre Content (Bagasse)

In contrast to the previous factors, increasing the proportion of sugarcane bagasse in the mixture showed a less linear and less pronounced impact. **Figure 6** illustrates the average thermal conductivity as a function of fibre percentage for different temperature (and/or thickness) levels.

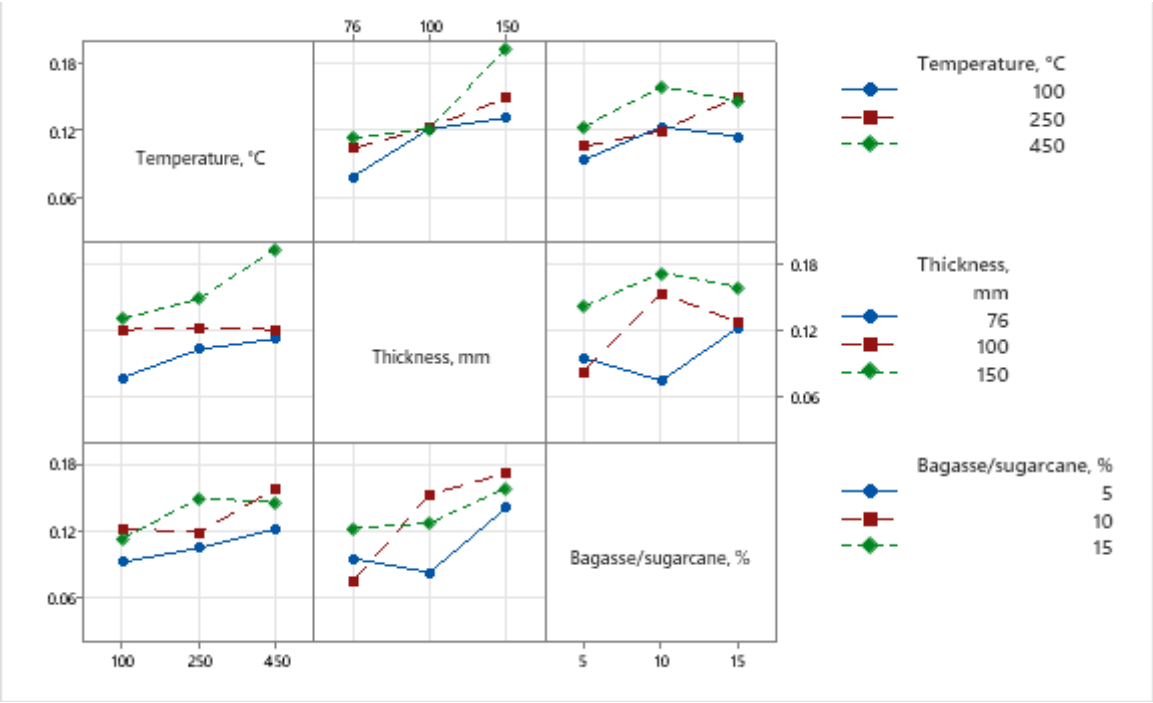

Figure 6. Thermal conductivity of diatomaceous earth versus the interaction effect among temperature, thickness, and bagasse percentage.

It can be observed that when increasing the bagasse content from 5% to 10%, k typically increases slightly, reaching a maximum around 10% fibre. However, going from 10% to 15%, in many cases, the change in k is not statistically significant, or even tends to decrease slightly.

For instance, at 250 °C, the blocks with 5% and 10% bagasse presented similar k values (~0.13–0.14 W/m·K), while increasing the content to 15% did not reduce con-

ductivity beyond the margin of error.

This non-monotonic response suggests the existence of an optimal fibre content (~10% by weight) where the reduction in density (and solid thermal path) is balanced with potential loss in structural continuity of the material. In fact, adding low to moderate amounts of fibre separates the diatomaceous particles more, potentially increasing porosity and lowering conductivity. However, adding too much fibre may lead to bridging or clumping, which can facilitate heat transfer or introduce discontinuities.

Another consideration is that bagasse fibre has its own thermal conductivity (~0.05–0.10 W/m·K, typical of dry lignocellulosic materials), so in small amounts it behaves more like an insulating filler within the diatomaceous matrix. However, at higher concentrations its contribution to conduction may no longer be negligible.

Increasing the bagasse content from 0 to 10% slightly raised k, while higher additions did not further improve insulation (not reducing k below ~0.12 W/m·K). This agrees with the initial hypothesis that fibres would not deteriorate conductivity, but rather moderate the rate of increase in k imposed by temperature.

3.4. Interactions Between Variables

The results suggest the existence of significant interactions among the factors. For instance, the effect of fibre depends on the levels of temperature and thickness. In **Figure 6**, it can be observed that for thinner blocks (76 mm) and across the tested temperature range, varying the bagasse content from 5% to 15% had virtually no effect on thermal conductivity (the curves are nearly flat). However, for thicker blocks (150 mm), the influence of bagasse content becomes more evident at high temperatures: at 150 mm and 450 °C, increasing bagasse beyond 10% appeared to reduce k instead of increasing it. Specifically, the k value at 150 mm and 450 °C dropped to approximately 0.18 W/m·K with 15% bagasse, compared to ~0.22 W/m·K with 10% bagasse under the same conditions.

This seemingly contradictory behaviour (reduction in k with more fibre only under certain conditions) may indicate that at high temperatures and in thick blocks, the fibre undergoes transformations (dehydration, thermal degradation) that alter the heat conduction structure. In any case, the temperature bagasse interaction proved significant, as confirmed by the ANOVA, implying that the effect of temperature on k is not independent of the fibre content.

Similarly, an interaction between temperature and thickness was detected, since the rate of increase of k with temperature varied depending on thickness, being more pronounced in thicker blocks (**Figure 5**). Finally, the interaction between thickness and bagasse appeared less relevant, although slight differences in trends may suggest that the optimal fibre content could vary slightly depending on block thickness.

3.5. Statistical Validation (ANOVA)

The three-factor analysis of variance quantitatively confirmed the previous observations. All main effects (A: temperature, B: bagasse content, C: thickness) were statistically significant ($p < 0.05$), confirming that each variable influences k within the studied range.

Regarding first-order interactions, the most significant was the A × B (temperature × bagasse) interaction, with $p < 0.05$, whereas the A × C (temperature × thickness) and B × C (bagasse × thickness) interactions showed less marked effects (p slightly > 0.05 in the linear model).

Additionally, significant curvature in the response with respect to temperature was detected: the quadratic term of temperature (A^2) in the fitted quadratic model was significant ($p < 0.01$), reflecting that the k(T) relationship is not purely linear, but tends to curve or saturate at high temperatures. The quadratic terms in B (fibre) and C (thickness) were not as significant, which aligns with a roughly linear behaviour of k with respect to these factors within the evaluated range.

Overall, the quadratic model adjusted using RSM produced an F-statistic of 18.3 (well above the critical value), indicating that the model is globally significant with a probability of less than 0.01% that the fit occurred by chance. The coefficient of determination was $R^2 \approx 0.95$ (estimated from the validation graph in **Figure 7**), indicating that the model explains the majority of the observed variability.

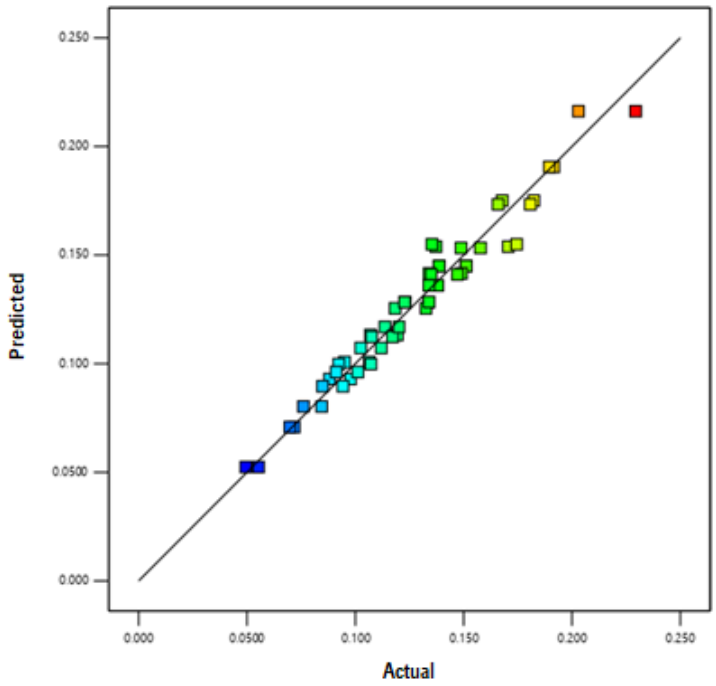

Figure 7. Scatter plot of predicted vs. actual thermal conductivity values. The close distribution of points along the identity line demonstrates the robustness of the fitted model.

Table 5 provides a graphical summary of the ANOVA (*p*-values for each term): it is evident that the three main factors and the quadratic term of temperature fall below the 0.05 threshold, whereas other interaction or quadratic terms do not offer significant improvements.

It is worth mentioning that the lack-of-fit test yielded a *p*-value of approximately 0.0748 (7.48%), slightly below the 10% threshold. This suggests that there may be a small systematic component not captured by the quadratic model (perhaps higher-order effects or heterogeneity), although in general the fit is acceptable for predictive purposes.

Table 5. Analysis of Variance (ANOVA) for the thermal conductivity coefficient as a function of heating surface temperature, block thickness, and bagasse content in the samples.

Source	Sum of Squares	df	Mean Square	F-Val.	*p*-value
Model	0.0731	26	0.00281	24.8	6.55E − 13
A-Temp.	0.0157	2	0.00787	69.4	2.30E − 11
B-Bagasse	0.00654	2	0.002327	28.8	1.99E − 07
C-Thickness	0.0287	2	0.0143	126	1.97E − 14
AB	0.00337	4	0.000358	7.43	0.000358
AC	0.00384	4	0.000145	8.47	0.000145
BC	0.0123	4	4.04E − 09	27.2	0.02
ABC	0.00258	8	0.02	0.02	-
Pure Error	0.00306	27	-	-	-
Total	0.0761	53	-	-	-

3.6. Empirical Model and Optimisation

Based on the RSM analysis, the following empirical equation for thermal conductivity [in units of W/(m·°C)] was obtained as a function of temperature (T in °C), block thickness (E in mm), and bagasse content (B in %), valid within the studied range (100 °C ≤ T ≤ 450 °C; 76 mm ≤ E ≤ 150 mm; 5% ≤ B ≤ 15%):

$$k(T, E, B) = 0.0996 + 4.11 \times 10^{-4}T + 3.28 \times 10^{-4}E + 1.17 \times 10^{-3}B - 4.07 \times 10^{-7}T^2 - 1.28 \times 10^{-6}T \cdot B$$

where only the statistically significant terms are included, and the coefficients can be refined with additional significant figures or variable coding.

This formula mathematically reflects the previously discussed trends: the positive coefficients for T, E, and B confirm that each factor increases thermal conductivity in a first approximation; the term $-4.07 \times 10^{-7}T^2$ indicates a negative curvature in the k(T) relationship (tendency to saturate); and the interaction term $-1.28 \times 10^{-6}T \cdot B$ shows that the combined effect of temperature and bagasse is negative (i.e., at higher temperatures, adding more bagasse may slightly reduce k, consistent with the negative sign of the co- efficient). This equation can be used to predict intermediate values of k and to optimise conditions.

For instance, by partially differentiating k with respect to each variable and identifying the theoretical minimum (**Figure 8**, contour plots), it was found that the optimal com- position within the studied range corresponds approximately to 10% bagasse, a temperature of ~250 °C, and a thickness of ~115 mm, reaching an estimated minimum thermal conductivity of approximately 0.13 W/(m·K).

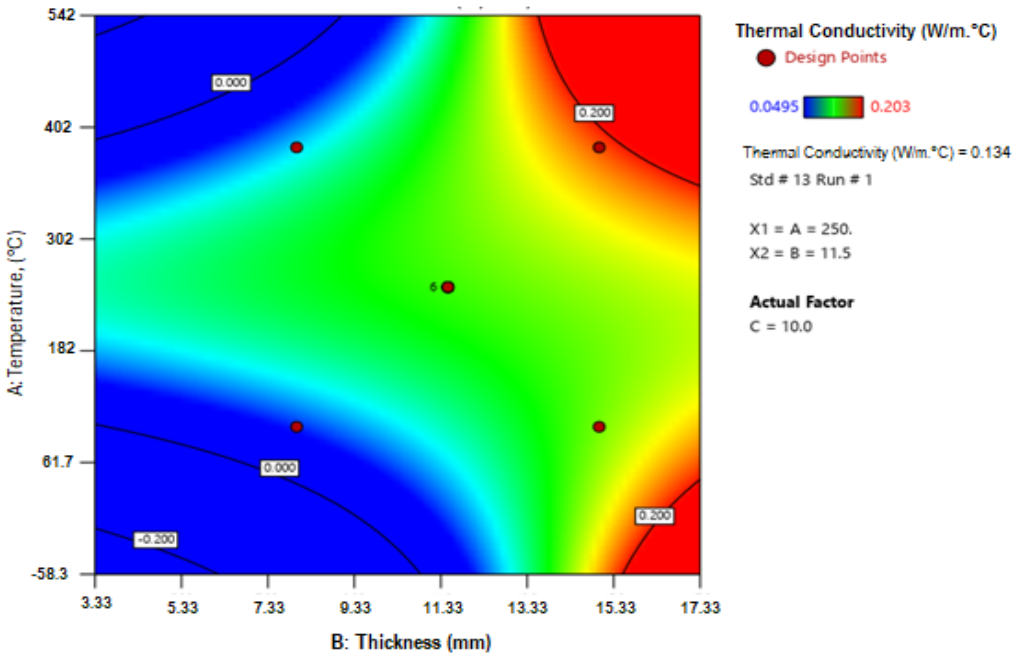

Figure 8. Contour plots of thermal conductivity for a sample containing 10% bagasse, considering the interaction between hot-surface temperature and block thickness. The optimal region is highlighted, with an average thermal conductivity of 0.134 W/(m·°C).

This result is consistent with the observation that 10% fibre represents a sweet spot and that lower temperatures tend to reduce conductivity. However, it should be noted that 0.13 W/(m·K) does not differ drastically from the average value of 0.125 W/(m·K), suggesting that within the explored design space, no combination dramatically reduces conductivity to values below 0.08 W/(m·K).

Figure 9 presents the 3D response surface for a specific case (bagasse content fixed at 10%), where the variation of k with T and E is visualised. The red points indicate the region of minimum k, located towards the lower-temperature and medium-thickness end. In fact, extrapolating be-

yond the original range, the model suggests that temperatures below 100°C and thicknesses under 76 mm would continue to reduce conductivity, possibly reaching values in the 0.05–0.07 W/(m·K) range (similar to lightweight insulation materials) if applied in thin panels and cold environments.

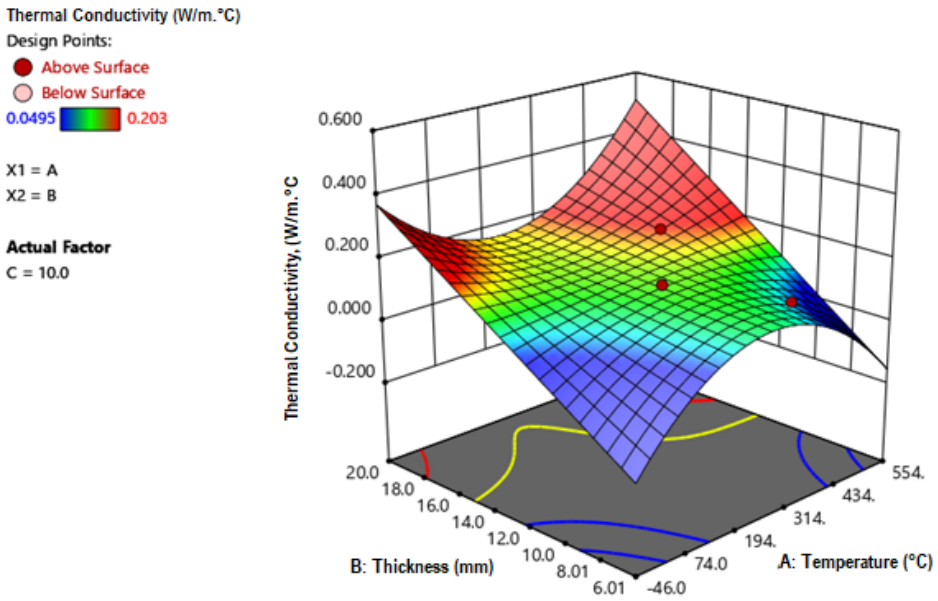

Figure 9. Three-dimensional representation of the response surface of thermal conductivity for a bagasse content of 10%, highlighting the optimal points under the interaction of temperature and block thickness.

On the other hand, the model also enables estimation outside the range: for example, for a very thick block (≥ 150 mm) with 15% bagasse at 500°C, it predicts k ~0.27 W/(m·K), which aligns with the slight increase trend observed experimentally under extreme temperatures.

3.7. Additional Results

Although the primary focus was on steady-state thermal conductivity, the research also examined transient behaviour and internal temperature distribution in selected cases. **Figure 10** shows the evolution over time of the temperature difference between the hot and cold faces of a block (10% bagasse, 50 mm thickness) subjected to a thermal jump. Initially, ΔT increases linearly with time until it approaches the steady-state regime, after which it stabilises and remains nearly constant. This indicates that during the heating process, the material's effective thermal conductivity changes (decreases) until a stable value is reached once thermal equilibrium is attained.

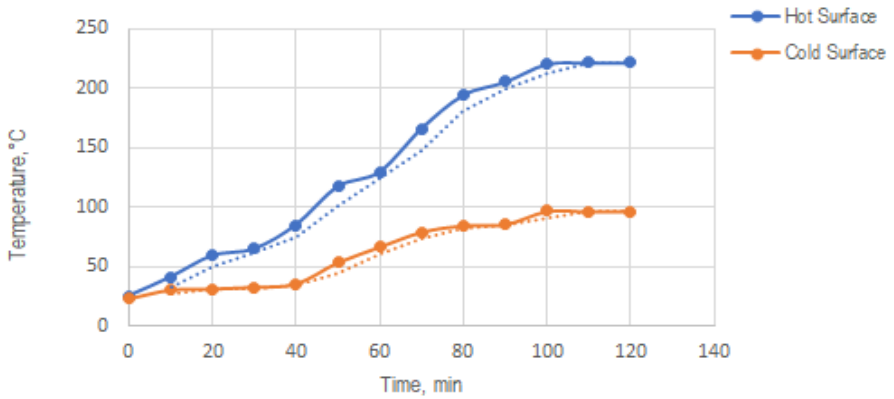

Figure 10. Thermal differential evolution in the transient regime for a sample with 10% bagasse content and 50 mm thickness. The temperature behaviour at the hot and cold surfaces is shown over a 120-minute test period.

Figure 11 presents the correlation between the hot surface temperature and the temperature recorded at the cold face for a 150 mm thick sample with 20% bagasse, as the former gradually increases from 23 °C to 500 °C. It can be observed that at lower input temperatures (< 100 °C), the output response is almost linear (indicating near-constant conductivity), but above 100 °C the curve deviates (logarithmic trend), tending towards thermal saturation where further increases in input temperature result in progressively smaller increases in output temperature. In fact, the correlation coefficient obtained was high (R2 = 0.9576), indicating a strong functional relationship between the inlet and outlet temperatures, albeit not strictly proportional. This supports the notion that the material approaches an asymptotic heat transfer regime at elevated temperatures.

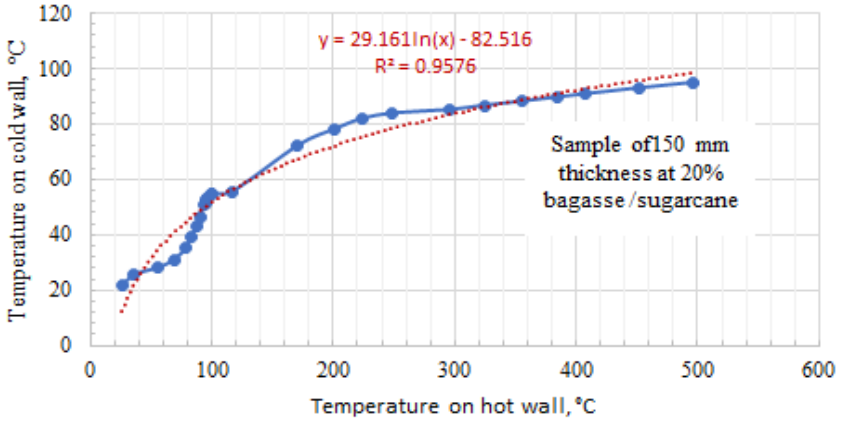

Figure 11. Relationship between the input temperature at the hot surface and the output temperature at the cold surface of a diatomaceous earth sample with 150 mm thickness and 20% bagasse. A logarithmic fit with high correlation is observed across the 23 °C to 500 °C range.

Figure 12 directly illustrates the variation in effective thermal conductivity versus measured temperature for the same case (150 mm block, 20% bagasse). Between 23 °C and 500 °C, conductivity increased only slightly from ~0.186 to ~0.267 W/(m·K), confirming that at very high temperatures, conductivity stabilises around ~0.25 W/(m·K). This finding is notable as, in many homogeneous materials, conductivity increases significantly with temperature (due to enhanced radiative and phonon contributions); in contrast, our composite material exhibits a pseudo-constant behaviour above 400 °C, likely attributable to internal changes such as the carbonisation of bagasse fibres forming micropores that offset the solid-phase conduction increase.

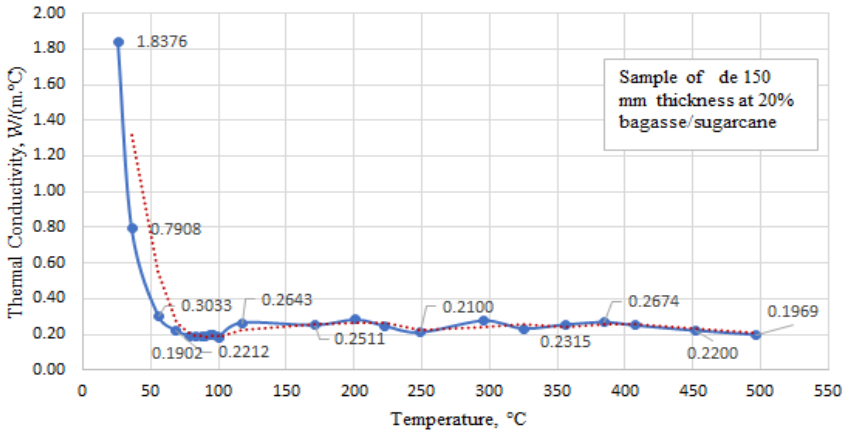

Figure 12. Thermal conductivity behaviour as a function of test temperature from 23 °C to 500 °C for a diatomaceous earth sample with 20% bagasse and 150 mm thickness. A sharp initial increase is followed by progressive stabilisation.

Finally, **Figure 13** shows the temperature profile along the thickness of the 150 mm, 20% bagasse sample under three hot-face conditions (500 °C, 250 °C, and 100 °C) at steady state. At 500 °C, a steep temperature drop is observed in the half closest to the heat source (a reduction of ~70% over the first ~75 mm), while the second half exhibits a gentler gradient (remaining 30% drop to ~95 °C at the cold face). In contrast, at 100 °C, the temperature drop is more evenly distributed (~27% reduction at mid-thickness, ~24% in the second half), with the cold face reaching approximately 55 °C. This implies that the thick block acts very efficiently as a thermal barrier at high temperature: even with 500 °C on one side, the opposite face barely exceeds 90–100 °C. In summary, these additional findings support the notion that the composite material performs in a stable and predictable manner under extreme conditions, and that its transient behaviour follows logarithmic patterns typical of porous materials (consistent with reports in the literature for composite solids).

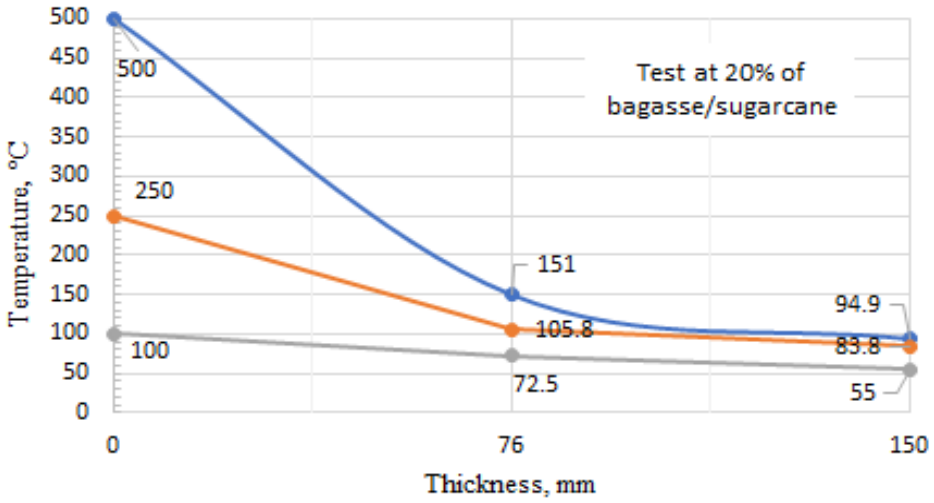

Figure 13. Thermal profile along the 150 mm thickness of a sample containing 20% bagasse under three hot-surface temperature levels (500 °C, 250 °C, and 100 °C). A progressive temperature drop towards the cold surface is observed, evidencing the composite material's thermal efficiency.

3.8. Comparative Assessment with Commercial Insulators

Table 6 presents a comparative summary of the thermal conductivity of the diatomite–bagasse composite and several conventional insulating materials. The results confirm that, although the composite exhibits a higher average thermal conductivity (~0.125 W/m·K) than premium insulators such as polymeric foams (~0.03–0.04 W/m·K) or mineral wools (~0.04–0.05 W/m·K), it remains structurally and functionally stable up to 500 °C. This feature is notable, since many conventional insulators lose their integrity at temperatures above 200–250 °C.

Table 6. Comparative thermal conductivity of the diatomite–bagasse composite and standard insulating materials.

Material	Thermal k (W m-1K-1)	Max. Temp. (°C)
Polystyrene foam	0.030–0.040	~80
Mineral wool	0.035–0.045	~250
Glass fibre	0.035–0.050	~250
Perlite (expanded)	0.040–0.060	~650
Calcium silicate	0.050–0.100	~1000
Diatomite–bagasse composite	**0.088–0.220 (avg. 0.125)**	**~500**

Therefore, the composite material may be particularly suitable for: (i) applications operating below 100 °C, such as refrigeration chambers, pipelines, and food storage systems; and (ii) medium-temperature systems (100–500 °C), where greater thicknesses can be adopted to compensate for its lower intrinsic conductivity, while still benefiting from its stability and low embodied energy.

4. Discussion

The above results demonstrate that the composite material of diatomaceous earth and sugarcane bagasse exhibits promising characteristics as a natural thermal insulator, albeit with some peculiarities in its thermal behaviour. Firstly, the average thermal conductivity obtained (~0.125 W/m·K) is higher than that of the most efficient commercial insulations (polymeric foams ~0.03 W/m·K, mineral wools ~0.04 W/m·K), and also higher than certain reported biocomposites, such as vegetable fibre panels (~0.05 W/m·K). This was expected, given that the diatomite used contains a significant amount of dense materials (silica, alumina), and the inclusion of 5–15% bagasse does not drastically reduce the block density.

This comparison is consistent with the data in **Table 6**, which highlights that the diatomite–bagasse composite occupies an intermediate niche between high-efficiency foams and mineral wools, and structural materials such as lightweight concrete. While not a premium insulator in terms of conductivity, its ability to remain stable up to 500 °C and its low embodied energy make it a viable solution for applications where high-temperature resistance and sustainability are prioritised over minimum conductivity. In particular, it can be applied to low-temperature insulation (< 100 °C) in refrigeration and storage, or to medium-temperature processes (100–500 °C) when larger thicknesses are implemented.

The studied composite can instead be classified as a medium-density insulator, comparable to cementitious mixes with lightweight aggregates. Indeed, a recent study reported conductivities of 0.128–0.152 W/m·K in mixtures based on expanded diatomite and perlite values very close to those found in this research, suggesting that it falls within the same order of magnitude as mineral-based insulation products used in construction. On the other hand, our composite offers important advantages: it utilises agricultural waste (bagasse) and a local mineral resource, without requiring high-temperature manufacturing processes or costly chemical additives. This implies lower production costs and lower embodied energy compared to synthetic or traditional ceramic insulations.

Moreover, although its thermal conductivity is higher than that of polystyrene foam, it remains relatively low compared to common structural materials, in fact, 3–5 times lower than that of lightweight concrete or adobe, which ranges from 0.4 to 0.6 W/m·K. In applications requiring high-temperature resistance or sustainability, this material could fill a useful niche.

A notable finding was the non-linearity in thermal response. Most homogeneous insulating materials show a roughly linear increase in k with temperature (due to the thermal excitation of heat carriers). However, this composite showed a trend towards saturation: beyond ~250–300 °C, the conductivity increased more slowly, and above 400 °C it appeared almost constant (0.25 W/m·K from 400 to 500 °C). This behaviour, contrary to conventional literature, may be explained by physicochemical changes in the material at high temperatures.

Bagasse fibre, composed of cellulose and hemicellulose, undergoes thermal degradation (pyrolysis) between 200–350°C, converting into fixed carbon (charcoal) and releasing volatiles. At ~450 °C, much of the fibre is likely to be carbonised, leaving a porous carbonaceous residue embedded within the diatomite matrix. Porous carbon has a relatively low thermal conductivity, potentially even lower than the original fibre, due to its high porosity. Additionally, the combustion of the fibre may generate further micro-cavities within the block, increasing the air fraction (a thermal insulator) in the microstructure. These combined factors could explain why, despite rising temperatures, heat transfer capacity does not escalate but instead stabilises.

It should be emphasised that the interpretations regarding pore formation and fibre carbonisation are based on indirect macroscopic evidence. In particular, the observed decrease in bulk density with block thickness reduction, together with the stabilisation of thermal conductivity at high temperature, strongly suggests an increase in porosity due to fibre degradation. Similarly, the transition in mechanical behaviour from ductile (as manufactured) to brittle (post-heating) aligns with the expected outcome of bagasse fibre carbonisation. Nevertheless, no direct microstructural evidence (SEM imaging or porosimetry) was collected in this initial stage. This limitation has now been explicitly ac-

knowledged, and detailed microstructural characterisation is identified as a logical and necessary step for future work.

In other words, at high temperatures, the material may become partially self-insulating due to fibre degradation, creating zones of low conductivity (pores, charcoal). This aligns with the observation that adding more than 10% fibre did not significantly decrease k, likely because the gain from increased porosity is offset by the fibre's inherent conductivity and compaction effects.

It is worth noting that it has been reported that in highly porous diatomite ceramics (85–90% porosity), conductivity at 200 °C can be as low as 0.06 W/m·K. Achieving such porosity in our blocks would require a higher content of foaming agents or similar processes, which may represent a future improvement path (e.g., adding more bagasse or pore-forming agents).

The observed increase in apparent conductivity with greater thickness warrants discussion, since k is theoretically independent of geometry. The rise in k with thicker samples may indicate internal gradients of moisture or temperature affecting the measurement. It is possible that the thicker blocks did not reach a fully uniform state during the test duration; despite waiting up to 4 hours, some inner regions may have retained residual moisture or lower temperatures, which would underestimate ΔT and artificially inflate k. Another possibility is thermal contact resistance: if thinner blocks conformed better to the plates (fewer irregularities), extra contact resistance in thicker ones might have reduced actual transfer, creating the illusion of higher intrinsic k. This type of experimental artefact is common in conductivity testing. To clarify, complementary tests using discs in a standard guarded hot plate apparatus (ASTM C177) are recommended to minimise contact error.

In practice, insulator thickness affects total thermal resistance (R = thickness/k); our finding suggests that at very large thicknesses, marginal efficiency might slightly decrease. That is, doubling thickness may not double resistance if k also increases slightly, yet insulation gains are still notable unless the curve fully flattens.

Regarding bagasse content, results suggest that it plays a secondary role in k magnitude but improves other properties. On the one hand, the fibre provides mechanical integrity: blocks with 0% bagasse were observed to be fragile and prone to cracking, whereas those with ≥ 5% fibre were manageable and more resistant to bending. This agrees with studies showing that plant fibres enhance the toughness of mineral matrices. On the other hand, the fibre is a renewable, economical organic resource that reduces block density (at 15% bagasse, dry density was ~850 kg/m^3, compared to ~1020 kg/m^3 with 0%). Lower density implies less stored heat (volumetric heat capacity), which is beneficial for fast thermal response. Indeed, during transient regimes, the fibre presence may have accelerated gradient stabilisation (lower thermal inertia).

Thus, although no dramatic k reduction was observed with fibre addition, the result is a lighter, more ductile and sustainable material. The fact that an optimum exists around 10% suggests that excessive fibre may hinder compaction or introduce defects (large pores), possibly allowing internal air convection at high temperatures. Future work may explore pre-carbonising the bagasse or using finer fibres to maximise insulation effects without exceeding 15%.

Comparing with updated international literature, our findings align with the trend of developing insulation composites from agro-industrial residues. In Chen et al. [12], biocomposites from agricultural cellulose and biodegradable polymers were developed to combine low conductivity with good mechanical properties. In fact, hybrid reinforcements of bagasse and crop residues in polymer matrices yielded conductivity reductions. Though focused on polymers, these works share the aim of valorising bagasse functionally.

In mineral-based systems, studies such as Dai et al. [22] improved foamed kaolin insulation by adding basalt fibres to lighten the product without sacrificing strength — a similar strategy to ours (replacing part of the solid phase with fibres). Likewise, Taoukil et al. [18] evaluated earth-fibre compounds and also observed non-linear temperature—conductivity behaviours due to fibre-induced anisotropy. This supports the idea that such non-linearity may be a general feature of anisotropic mineral—organic composites, considering that certain composite solids may exhibit inflections and peaks/minima in the conductivity—temperature curve, rather than monotonicity, due to phase or structural transitions. In our case, the "transition" could be fibre carbonisation, consistent with prior discussion.

A key strength of the material is its high-temperature resistance. Unlike most organic insulators (polyurethane, polystyrene, cellulose wool) that degrade above 200 °C, the diatomite–bagasse composite retained integrity and in-

sulating function up to 450–500 °C. This is primarily due to the refractory nature of diatomite (melting point > 1400 °C). Though bagasse burns at ~300 °C, its charred residue still limits conduction. Thus, the material could insulate medium-temperature systems (100–400 °C), where polymers fail and costly mineral wools are typically used.

Our results showed that even at 500 °C, the cold face of a 15 cm block remained below 100 °C—an impressive outcome. Properly installed, these blocks may line kilns, chimneys or dryers, provided mechanical integrity is maintained (as post-burning, the material may become friable). A possible enhancement would be incorporating an inorganic binder (e.g., clay or calcium aluminate cement) to reinforce the structure post-carbonisation. While this may slightly raise conductivity, it would be a practical trade-off.

In terms of sustainability and Peruvian applicability, this material fits the circular economy and earthen construction trends. Both Yapatera diatomite and sugarcane bagasse are local, renewable resources. Block manufacturing required no kilns (air-dried only) or complex industrial processes—unlike mineral wool (requiring > 1000 °C electric ovens) or synthetic foams (derived from petrochemicals). Its carbon footprint would be low; using bagasse retains carbon that would otherwise be released through agricultural burning.

It should be noted that the sustainability claims in this study are qualitative in nature. Our reasoning was based on the renewable origin of the raw materials (diatomite and agricultural bagasse) and on the comparatively low energy intensity of the fabrication process, which requires only air-drying instead of the high-temperature or petrochemical processing used for glass fibres, synthetic foams, or mineral wool. This indicates a preliminary environmental advantage, but does not constitute quantitative proof. To avoid overstatement, we have adjusted the wording in this manuscript to terms such as "potentially more sustainable" and "preliminary environmental benefit". A complete life-cycle assessment (LCA) and embodied energy calculation, which require extensive inventory data, are planned as a fundamental direction for our research group once the process is further optimised.

Socio-economically, a local production chain could be established where rural communities manufacture panels for thermally and acoustically insulated housing or artisanal thermal equipment. In warm regions, insulation reduces cooling needs, and in high-altitude zones, it can help retain indoor warmth. Our research provides initial design parameters—for example, a 5 cm panel would offer a thermal resistance $R \approx 0.50\ m^2 \cdot K/W$, sufficient to double the insulation of a typical adobe wall, improving thermal comfort.

Finally, certain limitations must be acknowledged. A key aspect is the potential influence of residual moisture. Both diatomaceous earth and sugarcane bagasse fibres are porous materials that can retain bound water, which may increase the apparent thermal conductivity, particularly in thicker blocks. In this initial study, the composite was tested in an "as-manufactured" state: the blocks had remained outdoors for three weeks prior to laboratory reception, and at the time of testing, they were visually and actually dry, with no evidence of free surface water. According to Peruvian building standards (RNE E.070–E.080 for adobe bricks) and ASTM D2216-19 (moisture content in soils), oven pre-drying is only mandatory when free moisture is present or when storage conditions could have altered the water content. Based on these criteria, oven drying was not applied in this campaign. Nevertheless, we recognise that eliminating the moisture variable is crucial for assessing the intrinsic behaviour of the material. Future work will therefore include oven-dried and desiccator-cooled samples to ensure fully dry reference conditions, allowing a more direct comparison with other insulating materials in the literature.

Additionally, the bagasse range should be expanded (0% to > 20%) to identify the inflection point where fibre excess compromises integrity. While qualitative observations indicated that blocks with ≥ 5% fibre exhibited improved handling and bending resistance compared to fibre-free specimens, no quantitative mechanical strength tests (e.g., compressive or flexural) were performed in this stage. Likewise, thermal cycling durability was not systematically evaluated, although preliminary inspection confirmed that the blocks maintained integrity up to 500 °C before becoming more brittle after fibre carbonisation. We recognise that these aspects are critical prerequisites for practical or commercial implementation. Therefore, comprehensive mechanical testing and repeated heating—cooling cycles are explicitly identified as essential next steps and will constitute a central focus of future research.

Lastly, cross-validating the methodology with direct conductivity tests (e.g., guarded hot plate apparatus on smaller specimens) would strengthen confidence in the absolute values reported.

This analysis is consistent with the results shown in **Figure 7**, which displays the predicted values from the fitted model against the actual thermal conductivity measurements. The strong alignment of the points along the 45-degree line indicates a high goodness-of-fit and validates the accuracy of the predictive model across the experimental domain.

Beyond the scope of this initial characterisation, future work will prioritise several research directions. Firstly, advanced microstructural characterisation (SEM and porosimetry) will be essential to visually and quantitatively confirm the pore formation and fibre carbonisation mechanisms inferred from macroscopic behaviour. Secondly, durability must be rigorously assessed through thermal cycling and hygrothermal ageing tests to quantify long-term stability under challenging environmental conditions. A full life-cycle assessment (LCA) will also be critical to support sustainability claims with robust quantitative evidence. Finally, optimisation of fabrication parameters and validation in specific applications (e.g., insulating panels or lightweight structural elements) will represent the final step for transferring this technology from laboratory scale to market readiness. These research directions are aligned with recent advances in sustainable composites from industrial by-products, cement—polymer hybrid systems, degraded cellulosic fibres, and lightweight concretes enhanced with waste-based materials as in Issarapanacheewin et al. [31] and El-Sayed et al. [32], which provide valuable insights into durability, environmental resistance, and performance optimisation.

In summary, the discussion confirms that the studied material performs its insulating function reasonably well and offers distinct advantages in specific contexts. It also reveals interesting non-linear behaviours that enrich our understanding of heat transfer in isotropic composite materials. This work lays the foundation for further optimisation (e.g., porosity enhancement or additives) and future research to develop eco-friendly thermal insulators from Peruvian resources, contributing to sustainability and local energy efficiency.

It is acknowledged that further studies employing SEM or porosimetry are required to confirm the pore structure evolution and the potential fibre carbonisation effects, providing deeper insight into the microstructural mechanisms underlying the observed thermal behaviour.

5. Conclusion

The main takeaways of this work are summarised concisely below:

1. The diatomaceous earth—bagasse composite exhibits an average thermal conductivity of ~0.125 W/(m·K) within the tested domain (100–450 °C, 76–150 mm, 5–15% wt. bagasse), while maintaining structural and functional stability up to ~500 °C.
2. Temperature and thickness significantly increase k (ANOVA, $p < 0.05$); the bagasse fraction has a weaker, non-monotonic influence with a practical optimum near ~10% by weight.
3. At high temperature (≈400 °C), k tends to plateau [~0.18–0.27 W/(m·K)], consistent with microstructural changes (fibre carbonisation and pore development) that counterbalance solid-phase conduction.
4. For design purposes, the thermal resistance $R = \Delta x/k$ confirms practical use: a 150 mm block provides $R \approx 1.20$ m2K/W, comparable to ~0.40 m of hollow ceramic brick and > 1.0 m of concrete to reach a similar R.
5. A quadratic response-surface model (with significant T, T2, and T × B terms) captures the behaviour with high goodness of fit ($R^2 \approx 0.95$) and is suitable for interpolation within the experimental ranges.
6. The material defines a niche proposition: a medium-performance, low-embodied-energy, and refractory natural insulator for the 100–500 °C window, based on locally available resources.
7. Limitations and next steps include: applying controlled compaction to quantify porosity effects, stricter moisture conditioning, cross-validation using a standard guarded hot-plate apparatus, and a techno-economic study (including break-even analysis).

Beyond these conclusions, it is important to emphasise that the microstructural interpretations presented here are based on indirect macroscopic evidence (density, conductivity, and mechanical behaviour). Direct confirmation through Scanning Electron Microscopy (SEM) and poro-

simetry was not within the scope of this first study, but it constitutes the next logical and priority step. Incorporating these techniques will allow unequivocal verification of pore morphology, fibre carbonisation effects, and their correlation with thermal and mechanical properties. This future characterisation will consolidate the present work as a foundational stage towards a comprehensive understanding and optimisation of diatomite–bagasse composites for sustainable insulation.

Finally, the present study did not include quantitative evaluation of mechanical strength or thermal cycling durability. These performance aspects are essential prerequisites for large-scale or commercial implementation and will form the central focus of forthcoming research. Comprehensive testing of compressive/flexural strength and repeated heating—cooling cycles will provide the necessary validation for long-term use in structural or industrial applications.

Author Contributions

Conceptualization, L.L. and A.H.; methodology, W.V. and L.L.; software, A.H.; validation, W.V. and L.L.; formal analysis, A.H.; investigation, W.V. and L.L.; resources, W.V. and L.L.; data curation, L.L.; writing—original draft preparation, A.H.; writing—review and editing, A.H.; visualization, A.H.; supervision, A.H.; project administration, A.H.; funding acquisition, W.V. and L.L. All authors have read and agreed to the published version of the manuscript.

Funding

This work was supported by the 2022 Teaching Research Projects Competition of Santo Toribio de Mogrovejo Catholic University (USAT), under grant number 1 under the title: "Adding Value to Sugar Cane Bagasse and Yapatera Diatomaceous Earth as a Composite Material for Thermal Insulation".

Institutional Review Board Statement

Not applicable.

Informed Consent Statement

Not applicable.

Data Availability Statement

The datasets generated and/or analysed during the current study are not publicly available, but they may be obtained from the corresponding author upon request.

Acknowledgments

The authors wish to express their appreciation to the academic staff and research administration at Santo Toribio de Mogrovejo Catholic University (USAT) for their invaluable technical support and institutional funding throughout the development of this study. Special thanks are extended to the School of Mechanical-Electrical Engineering for their assistance with control instruments and measurement tools, and to the Vice-Rectorate for Research, led at the time by Dr. Julio Hilario, for the financial support provided through the 2025 Research Projects Programme.

Conflicts of Interest

The authors declare that there is no conflict of interest.

Appendix A

Table A1. Full factorial 3 × 3 × 3 DOE matrix (extract).

Exp.	Temp. (°C)	Thick. (mm)	Bagasse (%)	k (W/m·K)
1	100	76	5	0.0845
2	250	76	5	0.0881
3	450	76	5	0.1194
4	100	76	5	0.07612
5	250	76	5	0.0978
6	450	76	5	0.1070
7	100	100	5	0.0943
8	250	100	5	0.1012

Table A1. *Cont.*

Exp.	Temp. (°C)	Thick. (mm)	Bagasse (%)	k (W/m·K)
9	450	100	5	0.1137
10	100	100	5	0.0849
11	250	100	5	0.0912
12	450	100	5	0.1202
13	100	150	5	0.1120
14	250	150	5	0.1184
15	450	150	5	0.1896
16	100	150	5	0.1025
17	250	150	5	0.1326
18	450	150	5	0.1916
19	100	76	10	0.0495
20	250	76	10	0.0698
21	450	76	10	0.0950
22	100	76	10	0.0554
23	250	76	10	0.0718
24	450	76	10	0.1064
25	100	100	10	0.1706
26	250	100	10	0.1341
27	450	100	10	0.1578
28	100	100	10	0.1490
29	250	100	10	0.1488
30	450	100	10	0.1578
31	100	150	10	0.1354
32	250	150	10	0.1381
33	450	150	10	0.2030
34	100	150	10	0.1745
35	250	150	10	0.1498
36	450	150	10	0.2294
37	100	76	15	0.0924
38	250	76	15	0.1388
39	450	76	15	0.1072
40	100	76	15	0.1072
41	250	76	15	0.1512
42	450	76	15	0.1387
43	100	100	15	0.1172
44	250	100	15	0.1228
45	450	100	15	0.1350
46	100	100	15	0.1075
47	250	100	15	0.1338
48	450	100	15	0.1472
49	100	150	15	0.1340
50	250	150	15	0.1678
51	450	150	15	0.1659
52	100	150	15	0.1229
53	250	150	15	0.1824
54	450	150	15	0.1808

References

[1] Cengel, Y.A., 2007. Heat and Mass Transfer: A Practical Approach, 3rd ed. McGraw-Hill: New York, NY, USA. (in Spanish)

[2] Holman, J.P., 2012. Experimental Methods for Engineers. McGraw-Hill: New York, NY, USA.

[3] Hahn, D.W., Ozisik, M.N., 2012. Heat Conduction, 3rd ed. John Wiley & Sons: Hoboken, NJ, USA.

[4] Incropera, F.P., DeWitt, D.P., Bergman, T.L., et al., 2008. Fundamentals of Heat Transfer. John Wiley & Sons: Hoboken, NJ, USA. (in Spanish)

[5] Bahadori, A., 2014. Thermal Insulation Handbook for the Oil, Gas, and Petrochemical Industry. Gulf Professional Publishing: Waltham, MA, USA.

[6] Abu-Jdayil, B., Mourad, A.-H.I., Hittini, W., et al., 2019. Traditional, State-of-the-Art, and Renewable Thermal Building Insulation Materials: An Overview. Construction and Building Materials. 214, 709–735. DOI: https://doi.org/10.1016/j.conbuildmat.2019.04.102

[7] Abdelrahman, M.A., Ahmad, A., 1991. Cost-Effective Use of Thermal Insulation in Hot Climates. Building and Environment. 26(2), 189–194. DOI: https://doi.org/10.1016/0360-1323(91)90026-8

[8] Guyer, E.C., Brownell, D.L., 1989. Handbook of Applied Thermal Design. Taylor & Francis: Philadelphia, PA, USA.

[9] Ige, J., Pilkington, P., Orme, J., et al., 2019. The Relationship Between Buildings and Health: A Systematic Review. Journal of Public Health. 41(2), e121–e132. DOI: https://doi.org/10.1093/pubmed/fdy138

[10] Panyakaew, S., Fotios, S., 2011. New Thermal Insulation Boards Made From Coconut Husk and Bagasse. Energy and Buildings. 43(7), 1732–1739. DOI: https://doi.org/10.1016/j.enbuild.2011.03.015

[11] Cai, G., Xu, Z., Li, W., et al., 2015. Experimental Investigation on the Thermal Protective Performance of Nonwoven Fabrics Made of High-Performance Fibers. Journal of Thermal Analysis and Calorimetry. 121, 627–632. DOI: https://doi.org/10.1007/s10973-015-4698-6

[12] Chen, J., Huang, Y., Deng, L., et al., 2023. Preparation and Research of PCL/Cellulose Composites: Cellulose Derived From Agricultural Wastes. International Journal of Biological Macromolecules. 235, 123785. DOI: https://doi.org/10.1016/j.ijbiomac.2023.123785

[13] Liu, X., Ai, Q., Zhou, H., et al., 2024. Influence of Fiber Topology on Anisotropic Thermal Conduction Properties of Composite Materials: A Cross-Scale Simulation Study. SSRN preprint. ssrn.4643152. DOI: https://doi.org/10.2139/ssrn.4643152

[14] Rudaz, C., Courson, R., Bonnet, L., et al., 2014. Aeropectin: Fully Biomass-Based Mechanically Strong and Thermal Superinsulating Aerogel. Biomacromolecules. 15(6), 2188–2195. DOI: https://doi.org/10.1021/bm500345u

[15] Zhang, X., Zhou, J., Wu, K., et al., 2024. Simultaneous Enhancement of Thermal Insulation and Impact Resistance in Transparent Bulk Composites. Advanced Materials. 36(16), 2311817. DOI: https://doi.org/10.1002/adma.202311817

[16] Ali, H., Dixit, S., Alarifi, S., 2024. Development and Characterization Study of Bagasse With Stubble Reinforced Polyester Hybrid Composite. Journal of King Saud University – Science. 36(7), 103231. DOI: https://doi.org/10.1016/j.jksus.2024.103231

[17] Kashcheev, I.D., Popov, A.G., Ivanov, S.E., 2009. Improving the Thermal Insulation of High-Temperature Furnaces by the Use of Diatomite. Refractories and Industrial Ceramics. 50, 98–100. DOI: https://doi.org/10.1007/s11148-009-9158-z

[18] Taoukil, D., El Meski, Y., Lahlaouti, M.I., et al., 2021. Effect of the Use of Diatomite as Partial Replacement of Sand on Thermal and Mechanical Properties of Mortars. Journal of Building Engineering. 42, 103038. DOI: https://doi.org/10.1016/j.jobe.2021.103038

[19] Verdeja, L.F., Ayala, J.M., Llavona, M.A., et al., 1993. Diatomites in Peru. Revista de Minas. 8, 121–129. (in Spanish)

[20] Modarresifar, F., Bingham, P.A., Jubb, G.A., 2016. Thermal Conductivity of Refractory Glass Fibres. Journal of Thermal Analysis and Calorimetry. 125, 35–44. DOI: https://doi.org/10.1007/s10973-016-5367-0

[21] Zapata, C.M., 2019. Use of Diatomite in the Production of Refractory Materials as Thermal Insulation in Industrial Processes [Bachelor Thesis]. Universidad Nacional de Piura: Piura, Peru. pp. 1–91. (in Spanish)

[22] Dai, H., Gao, H., Jiang, B., et al., 2024. Enhancement Effect of Basalt Fiber on the Foamy Kaolinite-Based Composite Thermal Insulator. Journal of Building Engineering. 95, 110144. DOI: https://doi.org/10.1016/j.jobe.2024.110144

[23] Sair, S., Mandili, B., Taqi, M., et al., 2019. Development of a New Eco-Friendly Composite Material Based on Gypsum Reinforced With a Mixture of Cork Fibre and Cardboard Waste for Building Thermal Insulation. Composites Communications. 16, 20–24. DOI: https://doi.org/10.1016/j.coco.2019.08.010

[24] Rein, P.W., 2017. Cane Sugar Engineering, 2nd ed. Verlag Dr. Albert Bartens KG: Berlin, Germany. DOI: https://doi.org/10.36961/cse

[25] Lobo-Ramos, L.L., Osorio-Oyola, Y.C., 2021. Comparative Study of the Thermal Conductivity of Three Natural Insulators with that of Expanded Polystyrene Calculated by Continuous Ice Melting [Bachelor Thesis]. Universidad Magdalena: Santa Marta, Colombia. pp. 38–51. (in Spanish)

[26] Villarreal-Albitres, W., 2005. An Experimental Investigation Into the Effect of Interface Friction on Bagasse Compaction Between Grooved Steel Plates [Master's Thesis]. James Cook University: North Queensland, Australia. pp. 1–186.

[27] Song, S., Lyu, Y., Zhao, J., et al., 2024. Broadband Sound Absorption Cellulose/Basalt Fiber Composite Paper With Excellent Thermal Insulation and Hydrophobic Properties. Industrial Crops and Products. 218, 118985. DOI: https://doi.org/10.1016/j.indcrop.2024.118985

[28] Yang, K., Zhang, Z., Liu, Y., et al., 2022. Biomass-Based Porous Composites With Heat Transfer Characteristics: Preparation, Performance and Evaluation — A Review. Journal of Porous Materials. 29, 1667–1687. DOI: https://doi.org/10.1007/s10934-022-01296-0

[29] Benavidez, E.R., Brandaleze, E., Lagorio, Y.S., et al., 2015. Thermal and Mechanical Properties of Commercial MgO-C Bricks. Matéria (Rio De Janeiro). 20(3), 571–579. DOI: https://doi.org/10.1590/S1517-707620150003.0058

[30] Freire-Lista, D.M., Fort, R., Varas-Muriel, M.J., 2016. Thermal Stress-Induced Microcracking in Building Granite. Engineering Geology. 206, 83–93. DOI: https://doi.org/10.1016/j.enggeo.2016.03.005

[31] Issarapanacheewin, S., Choomjun, D., Katekaew, W., et al., 2024. Leaching Behavior and Compressive Strength in the Immobilization of Cs-137 Contaminated Electric Arc Furnace Dust via Doping With Activated Carbon. Heliyon. 10(13), e33923. DOI: https://doi.org/10.1016/j.heliyon.2024.e33923

[32] El-Sayed, A.M., Faheim, A.A., Salman, A.A., et al., 2022. Sustainable Lightweight Concrete Made of Cement Kiln Dust and Liquefied Polystyrene Foam Improved With Other Waste Additives. Sustainability. 14(22), 15313. DOI: https://doi.org/10.3390/su142215313